Zefi, G., Ilioudis, C., Macdonald, M., & Clemente, C. (2024). A deceptive jamming technique against bistatic synthetic aperture radar. Paper presented at Microwave Remote Sensing: Data Processing and Applications III, Edinburgh, United Kingdom.

A deceptive jamming technique against bistatic SAR

Greta Zefi[a], Christos Ilioudis[a], Malcolm Macdonald[a], and Carmine Clemente[a]

[a]University of Strathclyde, Glasgow, UK

ABSTRACT

In recent years, radar jamming systems have become a crucial research area in the field of remote sensing for defence and security tasks. In a multistatic Synthetic Aperture Radar (SAR), the presence of false tagets created by a deceptive jammer is recognizable thanks to the presence of multiple receivers, whose positions might not be easily known by the jammer. In this configuration the bistatic SAR geometry can be designed so that false targets are kept out observed bistatic scene. In this paper, we propose a mathematical analysis that expresses the jammer's delay parameter as a function of the bistatic angle, identifying conditions to develop strategies to consistently induce the appearance of false targets in the bistatic scene and an analysis on how to place the false targets in the same position in the different bistatic images.

Keywords: Deceptive jammer, false targets, bistatic angle, bistatic SAR.

1. INTRODUCTION

Synthetic Aperture Radar (SAR) is a remote sensing technology that uses radar to create high-resolution images of the Earth's surface and provides day-and-night, weather-independent images.[1] Bistatic Synthetic Aperture Radar (BiSAR) is a SAR system whose transmitter and receiver are spatially separated. This separation improves the system's capability, reliability and flexibility, making it a promising and useful supplement to a classical monostatic SAR system. BiSAR has many advantages over the traditional monostatic SAR, including frequent monitoring, resolution enhancement, reduced vulnerability for military applications and reduced costs using existing illuminators of opportunity with several receive-only systems.[2] BiSAR have been widely investigated in many military and civilian remote sensing fields, such as reconnaissance, battlefield surveillance, change detection,.[3] In order to protect important facilities from detection and observation, the jamming methods against SAR and BiSAR have attracted many attentions and various jamming methods have been developed.[4]

Jamming methods can be broadly categorized into two types: barrage jamming[5,6] and deceptive jamming.[7] Barrage jamming involves emitting a signal to overpower the target's return, preventing the direct acquisition of the true SAR image.[5,6,8] On the other hand, deceptive jamming in SAR is achieved by capturing the transmitted signal, analyzing its relevant parameters, and subsequently re-emitting a jamming signal with similar characteristics, to generate false targets in the desired area in order to corrupt the SAR's image. A deceptive jammer intercepts the SAR's signal and re-transmits a delayed replica of the latter so that the SAR receives the false echoes and in the final image they will appear as false targets or deceptive scenes.[4,6,9]
Various methods have been presented in the literature such as,[9] where the authors present a new fast algorithm for large scene deceptive jamming against monostatic SAR, dividing the jamming scene into sub-templates based on focus depth, however without considering bistatic sensor configurations. While in[10] the authors present a jamming method for BiSAR that uses cosine phase modulation to create multiple false targets in both range and azimuth and in[11] they propose a jamming method against BiSAR based on frequency diversity array. With the use of multistatic SAR, deceptive jamming techniques become ineffective as false targets appear in different positions across the various bistatic maps. In this paper, we propose a method on how to place the false targets in the same position in the different bistatic images and a mathematical analysis that expresses the jammer's delay parameter as a function of the bistatic angle, identifying conditions in order to consistently induce the appearance of false targets in the bistatic scene.

Further author information: (Send correspondence to Greta Zefi)
Greta Zefi.: E-mail: greta.zefi@strath.ac.uk

2. DECEPTIVE JAMMING FOR BISAR

This section aims to clarify the different deceptive jamming techniques in bistatic SAR. In Sec. 2.1, the jamming signal model is introduced and described. In Sec. 2.2 the jammer's fixed time delay is presented and modeled. Finally, in Sec. 2.3 the variable jammer's time delay is presented in order to place false targets in desired positions.

2.1 Deceptive jamming signal model

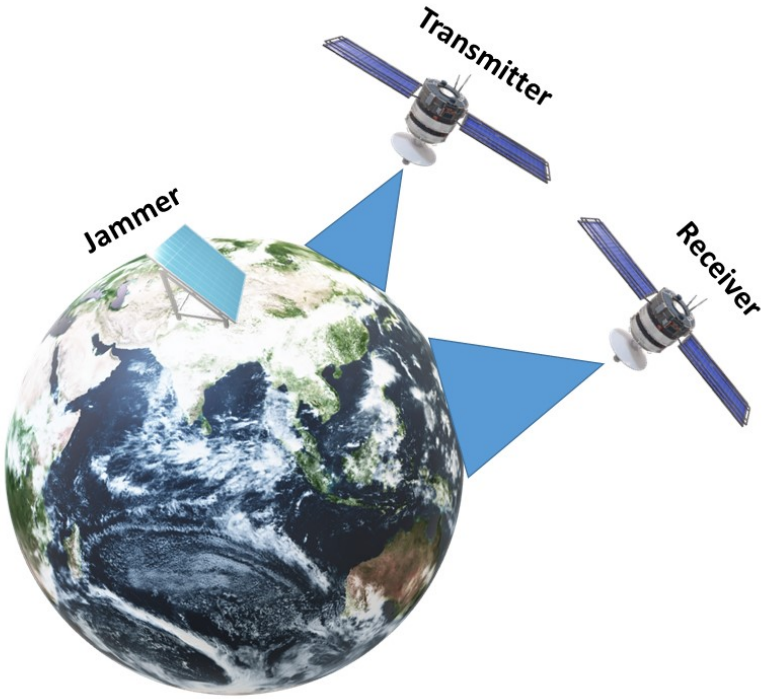

Figure 1: Bistatic SAR scenario in presence of a jammer.

Without loss of generality we assume that the transmitting antenna emits a linear frequency modulated signal (LFM) and the echoes received from the scene can be described as:

$$s_{rc}^{(i)}(t,\tau) = \omega_r\Big(\tau - \frac{R^{(i)}(t)}{c}\Big)\omega_a\Big(\frac{t}{T_a}\Big) \times e^{-j\frac{2\pi R^{(i)}(t)}{\lambda}} e^{j\pi K_r(\tau - \frac{R^{(i)}(t)}{c})^2} \tag{1}$$

Where τ is the fast-time domain, t is the azimuth time and T_a is the synthetic aperture duration, w_r and w_a are the range envelope function and azimuth envelope function respectively, c is the speed of light, K_r is the frequency modulation (FM) rate, λ is the wavelength. Furthermore, the range for the i-th receivers $R^{(i)}(t)$ is calculated as:

$$\begin{aligned} R^{(i)}(t) = &\sqrt{[x_R^{(i)}(t) - x_0]^2 + [y_R^{(i)}(t) - y_0]^2 + [z_R^{(i)}(t) - z_0]^2} \\ &+ \sqrt{[x_T(t) - x_0]^2 + [y_T(t) - y_0]^2 + [z_T(t) - z_0]^2} \end{aligned} \tag{2}$$

where (x_T, y_T, z_T) and $(x_R^{(i)}, y_R^{(i)}, z_R^{(i)})$ are the transmitter's and receivers' coordinates, respectively. In addition to the target echo, the jammer also emits a deceptive signal which is modelled as follows:

$$s_J^{(i)}(t,\tau) = w_r\Big(\tau - \frac{R_J^{(i)}(t)}{c} - \tau_{d_J}\Big)\omega_a\Big(\frac{t}{T_a}\Big) \times e^{-j\left(\frac{2\pi R_J^{(i)}(t)}{\lambda} + c\cdot\tau_{d_J}\right)} \cdot e^{j\pi K_r\left(\tau - \frac{R_J^{(i)}(t)}{c} - \tau_{d_J}\right)^2} \tag{3}$$

where τ_{d_J} is the time delay introduced by the deceptive jammer, which can be fixed or variable. The range history from the transmitter to the jammer and then from the jammer to the i-th receiver is:

$$R_J^{(i)}(t) = \sqrt{[x_R^{(i)}(t) - x_J]^2 + [y_R^{(i)}(t) - y_J]^2 + [z_R^{(i)}(t) - z_J]^2} + \sqrt{[x_T(t) - x_J]^2 + [y_T(t) - y_J]^2 + [z_T(t) - z_J]^2} \tag{4}$$

Therefore, the overall signal $s^{(i)}(t, \tau)$ at each receiver can be described as:

$$s^{(i)}(t, \tau) = s_{rc}^{(i)}(t, \tau) + s_J^{(i)}(t, \tau) \tag{5}$$

Hence all the receivers are jammed by the deceptive jammer and the false targets are generated in the multistatic SAR images.

2.2 Jammer's fixed time delay

The jammer emits a signal with a fixed delay which will appear as a focused target in a certain position (x_{ft}, y_{ft}, z_{ft}) in the monostatic SAR image, while in the bistatic SAR image the deceptive signal will appear as a focused target in different position depending on the receiver's location. If the receivers are located in different positions, there is the possibility that the introduced delay will correspond to a target outside the inspected scene.[12] In order to induce the constant presence of the false targets in the bistatic SAR images, the delay introduced by the jammer can be defined as follow:

$$\tau_{d_j} = \frac{B}{c}\left[\sin\theta_0 \cdot \frac{1}{\tan\frac{\beta_i}{2}} + \cos\theta_0\right] - \frac{R_J^{(i)}}{c} \tag{6}$$

where:

- β_i is the bistatic angle;
- B is the baseline, the distance between the transmitter and each receiver;
- θ_0 is the angle intercepted between the transmitter and the scene centre in azimuth domain.

2.3 Jammer's variable time delay

As discussed in the previous section, in order to place a false target in the same position on all BiSAR images, a different jamming signal delay must be applied at each SAR receiver. The proposed jamming pipeline is shown in Fig. 2. Analytically, starting from the jammer's position knowledge (see first block in Fig. 2), the jammer aims to estimate transmitter's and receivers' positions by using a tracking system (see second block). After estimating the position of the satellites, the jammer calculates the different delays that need to be emitted to different receivers (see third block), and explained by (8). In the fourth and fifth blocks, the different delays are sent by using a beam-forming system.[13] Specifically, in the Delay estimation block, the different delays are generated starting from the calculation of the different transmitter - false target - receiver distances as described below:

$$R_{ft}^{(i)} = \sqrt{[x_R^{(i)}(t) - x_{ft}]^2 + [y_R^{(i)}(t) - y_{ft}]^2 + [z_R^{(i)}(t) - z_{ft}]^2} + \sqrt{[x_T(t) - x_{ft}]^2 + [y_T(t) - y_{ft}]^2 + [z_T(t) - z_{ft}]^2} \tag{7}$$

In order to place a false target in the desired position (x_{ft}, y_{ft}, z_{ft}) in all the bistatic images, the delay that the jammer should add for the different receivers is:

$$\tau_{d_J}^{(i)} = \frac{R_{ft}^{(i)} - R_J^{(i)}}{c} \tag{8}$$

where the distance between transmitter - jammer - receiver, $R_J^{(i)}$, is described in equation (4).

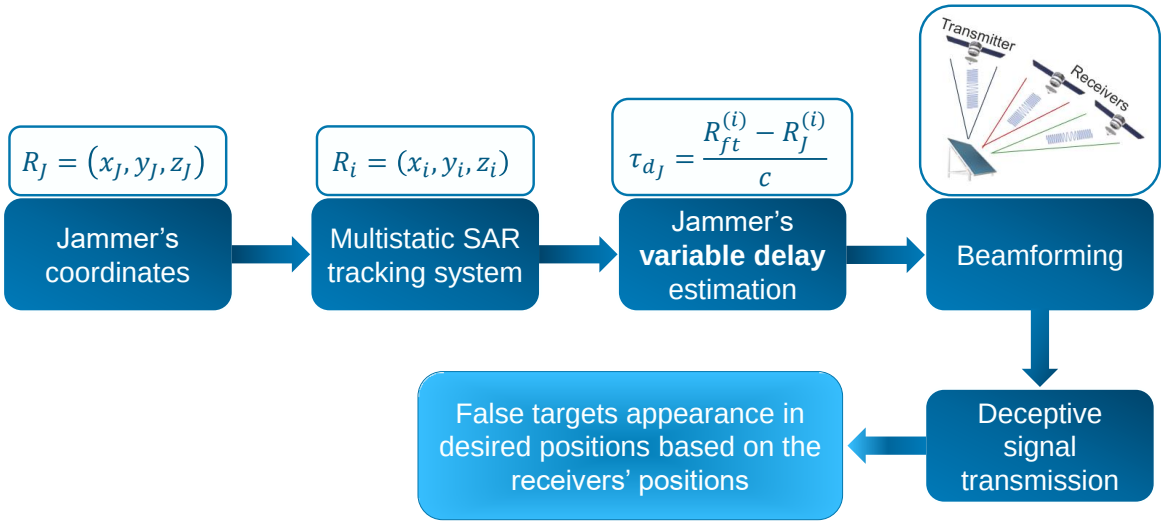

Figure 2: Signal processing chain block.

3. SIMULATION RESULTS

In this section, we illustrate how the analytical and qualitative discussions in the previous sections reflect the capability of the jammer to place false targets in the same position for each bistatic configuration. Specifically we simulated a spaceborne SAR scenario, one monostatic and two bistatics configurations. The three configurations operate in stripmap mode and the back-projection algorithm[14] is applied to process all the received echoes, see Fig. 4, 5. The reflectivity of the false targets and the real target is set to 1. The radar signal parameters are provided in Table 1 with the real target placed at $(0, 0, 0)$m. Additionally, 18 false targets are introduced, placed at different positions listed in Table 1. To emulate a scenario closer to the real-world case, we added a gaussian noise to the positions of the transmitter and receivers in order to simulate an uncertainty of a hypothetical tracking system (e.g., Extendend Kalman Filter, inspired by[15]) used to estimate the satellites' positions. Specifically, the noise used is as follows: $\mathcal{N}\ (0, \sigma_r^2) \in \mathbb{R}^3$, where σ_r is the estimation accuracy of the tracking system used to estimate the satellites' positions. To assess the functioning of our approach, we conducted a Montecarlo analysis[16] with different level of estimation accuracy σ_r. In particular, we evaluate our approach using the following values of the estimation accuracy $\sigma_r = [0.3, 1, 10, 20, 50, 100, 200, 500, 1000]$m and for each of these configurations we executed 1000 run tests. Note that, we started our analysis with $\sigma_r = 0.3$m based on the results obtained and described in.[17] Fig. 3 shows the result of the explained analysis, where on the x-axis we report σ_r and on the y-axis we report η_{err} that represents mean error of the false target position. The latter is defined as follows:

$$\eta_{err} = \mathbb{E}_{err}\left[\hat{R}_{ft} - R_{ft_{real}}\right] \tag{9}$$

We can notice from Fig. 3 a direct relationship between σ_r, η_{err} and σ_{err} that represents the error on the false target position with respect to the desired position (represented as error bar). In more detail, we can observe that as σ_r increases η_{err} and σ_{err} increases as well. We can notice as well, that the bistatic case, σ_{err} is higher than the monostatic case. This is because the bistatic case involves the estimation of both transmitter and receiver positions, which implies the sum of two uncertainties. Fig. 4a, 4b, 4c show the monostatic and two bistatic (TX-RX1, TX-RX2) images SAR with a real target in the center of the scenes and 18 false targets added with a fixed delay and Fig. 4d, 4e, 4f show the zoomed-in version around the false targets area.. The false targets appear distributed from position $x_{ft} = 75$m to $x_{ft} = 110$m in range and from $y_{ft} = 80$m to $y_{ft} = 100$m in azimuth in the monostatic image, while in the two bistatic images appear shifted as explained in.[12] In Fig. 5a, 5b, 5c are shown the monostatic and two bistatic (TX-RX1, TX-RX2) images SAR with a real target in the center of the scenes and 18 false targets distributed from position $x_{ft} = 75$m to $x_{ft} = 110$m in range and from $y_{ft} = 80$m to $y_{ft} = 100$m in azimuth and this is the designed/expected behavior and the

Table 1: Monostatic SAR, Bistatic SAR and Jammer parameters.

Transmitter	Receiver 1	Receiver 2	Jammer
$[-150, 0, 619]$km	$[-250, 5, 619]$km	$[-300, 8, 619]$km	$[600, 60, 0]$km
PRF	1500 Hz	T_{obs}	1 s
τ_T	10 μs	B_r	300 MHz
f_c	10 GHz	v	7500 $\frac{m}{s}$
false target 1	$(100, 100, 0)$m	false target 2	$(95, 100, 0)$m
false target 3	$(90, 100, 0)$m	false target 4	$(85, 100, 0)$m
false target 5	$(80, 100, 0)$m	false target 6	$(75, 100, 0)$m
false target 7	$(100, 90, 0)$m	false target 8	$(95, 90, 0)$m
false target 9	$(90, 90, 0)$m	false target 10	$(85, 90, 0)$m
false target 11	$(80, 90, 0)$m	false target 12	$(75, 90, 0)$m
false target 13	$(100, 80, 0)$m	false target 14	$(95, 80, 0)$m
false target 15	$(90, 80, 0)$m	false target 16	$(85, 80, 0)$m
false target 17	$(80, 80, 0)$m	false target 18	$(75, 80, 0)$m

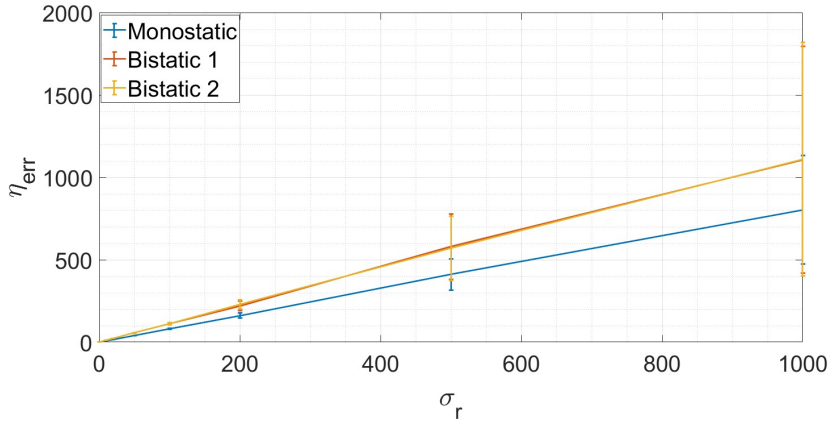

Figure 3: Mean error of the false target position as a function of the estimation accuracy of the satellites' positions. The plot represents the result of a Montecarlo analysis where 1000 run tests were conducted for each σ_r value. Specifically, the curves represent the mean error of the false target position calculated across the 1000 run tests and the error bars are the corresponding standard deviation.

proposed method has been simulated and a white Gaussian noise has been added. Fig. 5d, 5e, 5f show the zoomed-in version around the false targets area. From this analysis, we can observe that the actual position of the false targets is aligned with their desired positions specified in Table 1 with a standard deviation error of the false targets positions respectively: $\sigma_{err} = 5.6$m for the monostatic case and $\sigma_{err} = 8.1$m for the bistatic 1 and bistatic 2 cases for a $\sigma_r = 0.3$m. These results highlight the capability of our approach in positioning the false targets in the vicinity of the desired locations despite the presence of an error in the estimation of the satellites' positions. For completeness, the results for $\sigma_r = 500$m are also shown in Fig. 6a, 6b, 6c. It can be observed that the false targets shift from the desired position, and in the worst case, as in the analysis under consideration, the false targets do not appear in the observation scene. This result is due to the fact that, with an uncertainty of $\sigma_r = 500$m, the jammer is unable to place the false targets in the desired area. Consequently, the movement of the false targets in the image exhibits a significant error.

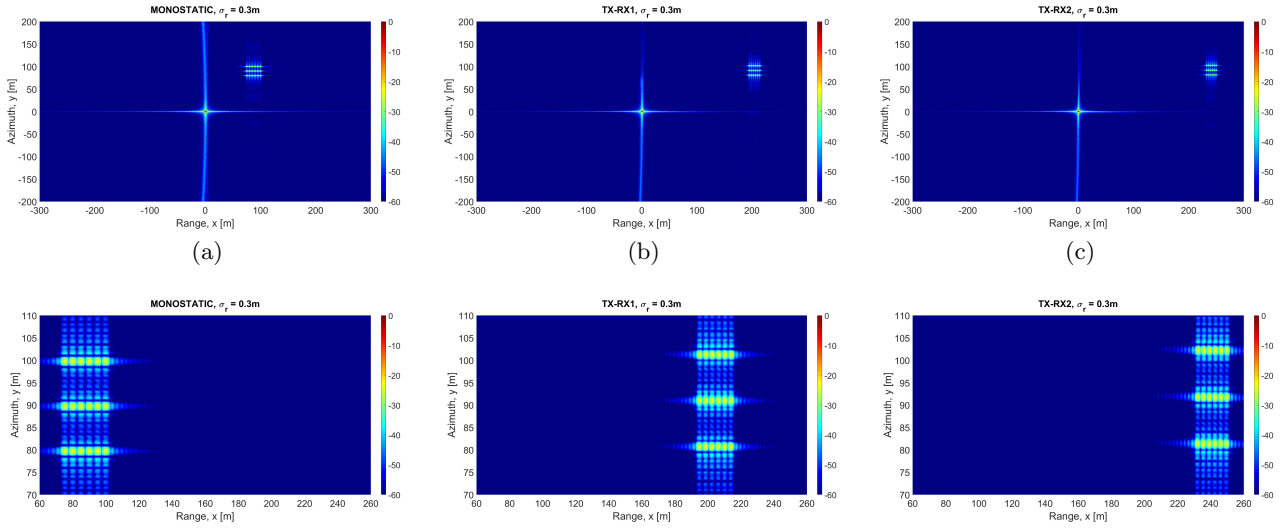

Figure 4: **Jammer's fixed time delay**. (a) **Monostatic configuration** and (b) its zoomed-in version around false targets; (c) **Bistatic configuration 1** and (d) its zoomed-in version around false targets; (e) **Bistatic configuration 2** and (f) its zoomed-in version around false targets. In this experimental settings, $\sigma_r = 0.3$m.

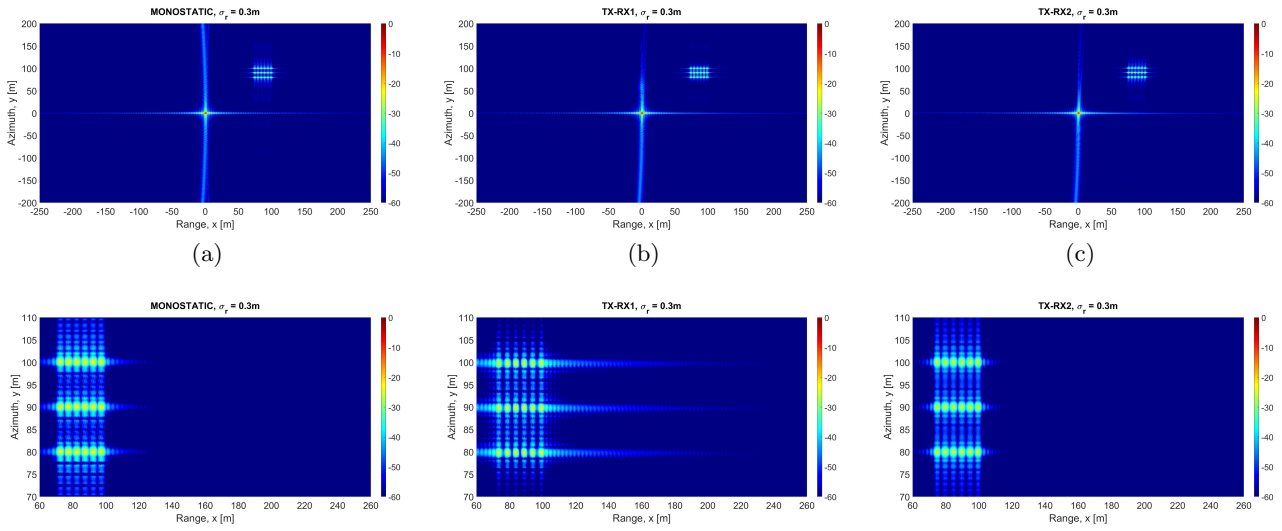

Figure 5: **Jammer's variable time delay**.(a) **Monostatic configuration** and (b) its zoomed-in version around false targets; (c) **Bistatic configuration 1** and (d) its zoomed-in version around false targets; (e) **Bistatic configuration 2** and (f) its zoomed-in version around false targets. In this experimental settings, $\sigma_r = 0.3$m.

4. CONCLUSIONS

In this paper, we investigate the problem of deceptive jamming in bistatic SAR, identifying a method on how to locate false targets in the same positions for the different bistatic images. To do this, we present a complete pipeline that calculates different time delays for each receiver and emits different signals considering these various time delays using a beamforming technique. As result, we are able to obtain false targets in the same positions across the various bistatic images. Nonetheless, possessing accurate knowledge of the satellites' positions is crucial, even with a variable delay, as the latter, while more robust, still requires precise positional information.

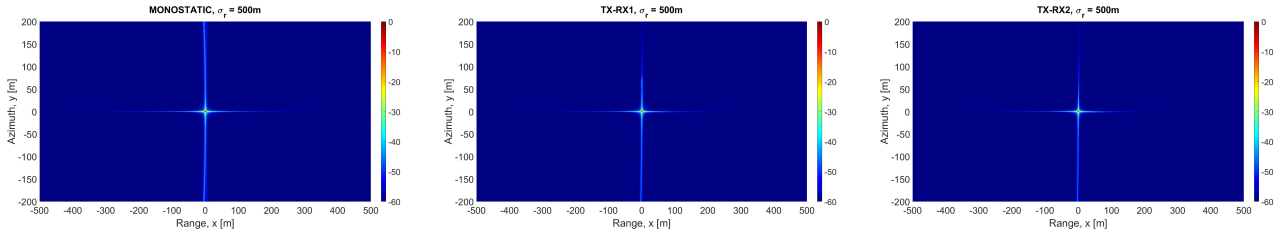

(a) (b) (c)

Figure 6: **Jammer's variable time delay with $\sigma_r = 500$m.**(a) **Monostatic configuration**, (b) **Bistatic configuration 1**, (c) **Bistatic configuration 2**

Future work will be devoted to assess the behavior of our approach in real-world setting.

ACKNOWLEDGMENTS

This work is supported by DSTL under the project entitled "Advanced Imaging Algorithms for Distributed Spaceborne SAR.

REFERENCES

[1] Moreira, A., Prats-Iraola, P., Younis, M., Krieger, G., Hajnsek, I., and Papathanassiou, K. P., "A tutorial on synthetic aperture radar," *IEEE Geoscience and remote sensing magazine* **1**(1), 6–43 (2013).

[2] Walterscheid, I., Ender, J. H., Brenner, A. R., and Loffeld, O., "Bistatic sar processing and experiments," *IEEE Transactions on Geoscience and Remote Sensing* **44**(10), 2710–2717 (2006).

[3] Liu, F., Antoniou, M., Zeng, Z., and Cherniakov, M., "Coherent change detection using passive gnss-based bsar: Experimental proof of concept," *IEEE transactions on geoscience and remote sensing* **51**(8), 4544–4555 (2013).

[4] Sun, Q., Shu, T., Yu, K.-B., and Yu, W., "Efficient deceptive jamming method of static and moving targets against sar," *IEEE Sensors Journal* **18**(9), 3610–3618 (2018).

[5] Dumper, K., Cooper, P., Wons, A., Condley, C., and Tully, P., "Spaceborne synthetic aperture radar and noise jamming," in [*Radar 97 (Conf. Publ. No. 449)*], 411–414 (1997).

[6] Liu, Q., Xing, S., Wang, X., Dong, J., and Dai, D., "A strip-map sar coherent jammer structure utilizing periodic modulation technology," *Progress In Electromagnetics Research B* **28**, 111–128 (2011).

[7] Long, S., Hong-rong, Z., Yue-sheng, T., and Chang-yao, Z., "Research on deceptive jamming technologies against sar," in [*2009 2nd Asian-Pacific Conference on Synthetic Aperture Radar*], 521–525, IEEE (2009).

[8] Zhang, J., Dai, D., Xing, S., Xiao, S., and Pang, B., "A novel barrage repeater jamming against sar-gmti," in [*2016 10th European Conference on Antennas and Propagation (EuCAP)*], 1–5, IEEE (2016).

[9] Zhou, F., Zhao, B., Tao, M., Bai, X., Chen, B., and Sun, G., "A large scene deceptive jamming method for space-borne sar," *IEEE Transactions on Geoscience and Remote Sensing* **51**(8), 4486–4495 (2013).

[10] Jinhe, R., Xiuhe, L., and Yang, S., "A jamming method against bistatic sar based on modulation theory," *Journal of Systems Engineering and Electronics* **30**(3), 504–510 (2019).

[11] Huang, B., Nusenu, S. Y., Zhang, S., Wang, W.-Q., Liao, Y., and Wang, Z., "A deceptive jamming against high and low orbit bistatic sar using frequency diversity array," in [*2019 6th Asia-Pacific Conference on Synthetic Aperture Radar (APSAR)*], 1–5, IEEE (2019).

[12] Zefi, G., Ilioudis, C., Macdonald, M., and Clemente, C., "Analysis of deceptive jamming in multistatic sar," in [*IGARSS 2024-2024 IEEE International Geoscience and Remote Sensing Symposium*], 11437–11441, IEEE (2024).

[13] Barton, P., "Digital beam forming for radar," in [*IEE Proceedings F (Communications, Radar and Signal Processing)*], **127**(4), 266–277, IET (1980).

[14] Ding, Y. and Munson, D. J., "A fast back-projection algorithm for bistatic sar imaging," in [*Proceedings. International Conference on Image Processing*], **2**, II–II, IEEE (2002).

[15] Coelho, M. d. F., Bousson, K., and Ahmed, K., "An improved extended kalman filter for radar tracking of satellite trajectories," *Designs* **5**(3), 54 (2021).

[16] Rubinstein, R. Y. and Kroese, D. P., [*Simulation and the Monte Carlo method*], John Wiley & Sons (2016).

[17] Elisha, Y., Shyldkrot, H., and Hankin, M., "Orbit determination system for low earth orbit satellites," in [*Proceedings of the 20th International Symposium on Space Flight Dynamics*], (2007).